



# Betanin-encapsulated starch nanoparticles: synthesis and cytotoxic effect on colon cancer

Suhail Ahmad Bhat<sup>1</sup> · Sathyapriya Chandramohan<sup>1</sup> · Guguloth Sai Krishna<sup>1</sup> · Chandansri Hiranmaya<sup>1</sup> · Sankar Pajaniradje<sup>1</sup> · Anjali Suresh Nair<sup>1</sup> · Debabrata Mohanty<sup>1</sup> · Rukkumani Rajagopalan<sup>1</sup>

Received: 3 March 2024 / Accepted: 1 September 2024  
© King Abdulaziz City for Science and Technology 2024

## Abstract

Colorectal cancer (CRC) is a common and life-threatening neoplastic disease that continues to pose a formidable challenge to global health. The present work was performed to evaluate the anticancer properties of betanin and betanin (BT) loaded starch nanoparticles (S-BT). The BT and S-BT were characterized by DLS, SEM, UV spectroscopy, XPS and FTIR. The cytotoxic effect was assessed by MTT and LDH assay. The apoptotic potential of BT and S-BT was assessed by DCFDA, Rh123, AO/EB and DAPI staining methods. Cell cycle arrest was depicted using flow cytometry. The antimetastatic potential of BT and S-BT was evaluated by wound healing assay. The S-BT showed a spherical morphology with a size of 175 nm. The betanin contained SNPs were found to have strong encapsulation efficiency and favorable release profiles. Both BT and S-BT exhibited cytotoxicity in SW480 cells but S-BT displayed increased cytotoxicity when compared to BT alone. Loss of mitochondrial membrane potential, nuclear fragmentation, chromatin condensation and generation of ROS, all indicative of apoptotic mode of cell death, were revealed by fluorescence imaging. The cells were arrested in the G<sub>2</sub>M phase. Moreover, both BT and S-BT were able to inhibit the migratory potential of SW480 cells. Overall, our results indicated that both BT and S-BT were able to induce anticancer effects; and, S-BT was found to have increased therapeutic efficacy when compared to BT alone.

**Keywords** Colorectal cancer · Starch nanoparticles · Betanin · Sustained release · MTT · ROS induction

Suhail Ahmad Bhat and Sathyapriya Chandramohan have contributed equally to this work and share first authorship.

✉ Rukkumani Rajagopalan  
ruks2k2@gmail.com; rrlabs2011@gmail.com

Suhail Ahmad Bhat  
sabhat666@gmail.com

Sathyapriya Chandramohan  
sathyapriyachandramohan@gmail.com

Guguloth Sai Krishna  
gskrishna\_9@pondiuni.ac.in

Chandansri Hiranmaya  
chiranmaya99@gmail.com

Sankar Pajaniradje  
sankar86in@gmail.com

Anjali Suresh Nair  
anjalisnair.3209@gmail.com

Debabrata Mohanty  
debabrata14319@gmail.com

<sup>1</sup> Department of Biochemistry and Molecular Biology, School of Life Sciences, Pondicherry University, Puducherry 605014, India

## Introduction

Cancer is a complex and multifaceted disease that involves a wide range of bodily processes in its progression (Richon et al. 1998). The worldwide incidence of cancer is still rising despite tremendous progress in understanding its causes. The prevalence and impact of this disease were highlighted in the statistics released by the World Health Organisation in 2018 (Chen et al. 2021; Pains et al. 2015).

With colorectal cancer (CRC) accounting for 9.4% of cancer-related deaths in 2020, it is the second deadliest and third most common cancer globally. It is predicted that by 2035, the incidence of this serious global health concern will be quadrupled worldwide, with significant increase in less developed nations. CRC risk factors include diet, lifestyle, and genetics. Many countries have population-based screening programmes in place as they are the most effective preventive measure. Early identification is crucial because of the slow growth of CRC. Despite the challenges associated with chemotherapy, early intervention and addressing risk factors are essential in the fight against colorectal cancer

(Aztatzi-Ruggerio et al. 2019). Colorectal cancer (CRC) is caused by a variety of pathways, each with its own precursors and risks. These pathways include microsatellite instability, chromosomal instability, and serrated neoplasia. The most common type of colorectal cancer, adenocarcinoma, has different treatments depending on the disease's stage as it progresses from benign polyps to invasive malignancy (Wlodkovic et al. 2011). Surgery is often used in the early stages, but additional therapies are required in the later stages, and the full extent of recovery is still unknown (Pickhardt et al. 2013). The use of chemotherapy and targeted medications such as angiogenesis inhibitors and anti-EGFR drugs has completely changed the way colorectal cancer is treated (Sreekanth et al. 2007). Promising research are being conducted on gene therapy and immunotherapy, including adaptive T-cell treatment, cancer vaccines, immune checkpoint inhibitors, monoclonal antibody therapy, complement inhibition, cytokine therapy, and natural products. These methods seek to increase the effectiveness, lessen adverse effects, and improve CRC treatment (Aztatzi-Ruggerio et al. 2019).

The development of highly effective drug delivery technology called nanoencapsulation has transformed cancer treatment and made a variety of nanoformulations of chemotherapy available (Hossain et al. 2022; Mourdikoudis et al. 2018; Otto and Sicinski 2017; Siegel et al. 2020; Xie et al. 2020). Polysaccharides, mainly starch, have the potential to prevent nonspecific protein adsorption and allow for a variety of modifications, making them promising agent for drug delivery (Chen et al. 2022; Contreras-Cáceres et al. 2019; Jimenez et al. 2000; Lu et al. 2018; Wu et al. 2016). Although histone deacetylase inhibitors, such as CG-1521, have the potential to treat colon cancer, their solubility and metabolism present challenges that call for creative solutions (Salimi et al. 2021; Zaremba-Czogalla et al. 2020). The betanin from beetroot demonstrates strong antioxidant and anticancer property, indicating its potential for use in cancer treatment (Bray et al. 2018; Pang et al. 2015). Betanin has been shown to have antioxidant activity in biological lipid domains in human macromolecules such as low-density lipoproteins, entire cells, and membranes (da Silva et al. 2019). Furthermore, because of its anti-inflammatory and hepatic safety properties in whole human cells, betanin has aroused the curiosity of researchers (Khan 2015). This protein affects the redox-mediated signal transduction pathways involved in inflammatory responses in cultured endothelial cells, and betanin also showed antiproliferative effects on human cancer cell lines (Kapadia et al. 2011). The primary goal of this research was to demonstrate betanin's potential as an anti-cancer medication for the treatment of cancer by examining its cytotoxic and anti-metastatic effects in SW480 cells.

## Experimental procedures

### Materials and methods

#### Chemicals

All the reagents were procured from Sigma Aldrich, India: Betanin, DAPI stain, sodium hydroxide pellets, and Rhodamine 123. Dulbecco's modified eagle medium (DMEM), MTT, acridine orange, ethidium bromide, propidium iodide, Bradford reagent, acetic acid, methanol, Proteinase-K, RNase, ethanol, Polysorbate 80, Triton X-100, and foetal bovine serum (FBS) were obtained from HiMedia, India. Merck, India supplied the acetone. All cell culture equipments, including flasks and well plates, complied with cell culture guidelines and additional laboratory necessities used were of the molecular grade.

#### Synthesis of starch nanoparticles (SNPs)

The nanoparticle was synthesized using the ultra-sonication method. In brief, 5 g of starch was dissolved in 0.1 N NaOH and sonicated in an ultra sonicator for 10 min with AMP 80% and pulse 02/02. After sonication, 600 µl of tween 80 was added and again sonicated with same AMP and time. Under the process of sonication, 10 ml of absolute ethanol was added dropwise for 10 min. The final sample obtained was kept closed for overnight and allowed to get precipitated. After 12 h of incubation, the precipitate obtained were SNPs. The synthesized SNPs were stored at 4 °C for further use.

#### Encapsulation of betanin in SNP

Encapsulation procedure was carried out by gelatinizing the SNPs with the help of NaOH. 5 g of SNPs were added to 30 ml of 0.4 M sodium hydroxide. Gelatinization process was carried out by heating the solution in 80 °C for 20 min. The solution was kept in room temperature until a dense solution is observed and kept for cooling. Betanin was prepared in 5 ml of MilliQ water (300 mg of betanin in 10 ml). Before adding drug into the gelatinized starch, the dense solution was kept under continuous stirring at 60 °C. The betanin solution was added dropwise and allowed to precipitate by adding 20 ml of acetone. The stirring was stopped after 12 h and the centrifugation was carried out at 1000 rpm in room temperature for 20 min. The supernatant obtained was stored and used for drug loading estimation. The precipitate obtained was washed with 5 ml of acetone and lyophilized.

## Physiological characterization of the betanin-loaded SNPs

### Particle size analysis

Particle size analysis was performed for the encapsulated betanin (S-BT) suspended in Mili-Q using a Zetasizer™ (Malvern Instruments, UK) system, configured at 25 °C, 347.8 kcps count rate, and 1.50 material refractive index.

### Ultraviolet absorbance spectrum

UV study was conducted for betanin (BT), S-BT, with Mili-Q as the solvent using a UV-1700 Shimadzu UV visible spectrophotometer. We examined the absorbance maxima between 400 and 800 nm wavelength range.

### SEM imaging

SEM imaging of the betanin encapsulated NPs was done by subjecting the sample to the Scanning electron microscope. Images were taken by focusing in particular area in 10× autofocus.

### X-ray diffraction (XRD)

The accurate characterization of a material's crystallographic arrangement, chemical composition and physical attributes can be achieved using the non-invasive methodology of X-ray diffraction analysis (XRD). In order to elucidate the structural configuration of S-BT, X-ray diffraction analysis was employed on the S-BT specimen.

### X-ray photoelectron spectroscopy (XPS) and Fourier transform infrared spectroscopy (FTIR)

Encapsulated Starch Nanoparticles were subjected to an elemental analyzer. The percentage of carbon and oxygen in the samples was obtained and analyzed to draw inferences about the possibility of successful drug encapsulation. The Fourier transform infrared spectra of empty starch nanoparticles and S-BT was performed to determine their functional groups. The FTIR spectrum was recorded over a range of 500–4500  $\text{cm}^{-1}$  with Kbr as a reference (Thermo Scientific Nicolet 6700 spectrometer).

### In vitro release study

A drug release study was conducted by using the dissolution technique. In summary, 10 kDa molecular weight cut-off dialysis membranes contained a known quantity of drug-loaded nanoparticles (NPs). After that, the dialysis bag was continuously stirred or agitated in the PBS solution (PH 7.4)

for 120 h at 37 °C. A known amount of the solution was taken and replaced with new solvent at the designated intervals. The standard curve was used to calculate the drug's concentration after it was released.

### Encapsulation efficiency (%EE) and drug loading

UV–Vis spectrometry was used to calculate the percentage of encapsulation efficiency (% EE). The content of the drug was calculated as follows; about 2 mg of S-BT was dispersed in 10 ml of milliQ water and centrifuged for 10,000 rpm for 10 min. During the washing-centrifugation step, the supernatant of the NPs suspension was collected and the concentration of betanin (BT) was measured to estimate the free drug. The following formulas were used to calculate the percentage EE. The weight of the NPs was calculated from the NP yield in order to estimate the percentage loading content (%LC). The following formulas were used to calculate the percentages of LC and EE.

$$\%EE = \frac{[(\text{Drug added} - \text{Free "untrapped drug"}) / \text{Drug added}] * 100}{}$$

$$\%LC = [\text{Entrapped drug} / \text{nanoparticles weight}] * 10$$

## Anticancer study

### Cell lines and culture conditions

From NCCS (Pune), India, SW480 cell lines were acquired. In an environment of 5%  $\text{CO}_2$  and 95% humidified air, the cancer cell lines were grown at 37 °C in a  $\text{CO}_2$  incubator using Dulbecco's Modification of Eagle's Medium (DMEM) supplemented with 10% foetal bovine serum (FBS), 50  $\mu\text{g}/\text{ml}$  penicillin, and 50  $\mu\text{g}/\text{ml}$  streptomycin. SW480 cells were routinely sub-cultured in tissue culture flasks in order to maintain their viability. Cells were splitted upon reaching confluency and the culture medium was replaced every 48 h.

### Cell viability/cytotoxicity assay

The viability of cells following treatment with both free and nano-encapsulated drugs was assessed using the MTT colorimetric assay. In brief, actively proliferating SW480 cells were plated onto the flat-bottom 96-well plates at a density of approximately  $6 \times 10^3$  cells per well in Dulbecco's Modified Eagle Medium (DMEM) supplemented with 10% foetal bovine serum (FBS). Subsequently, the plates were incubated at 37 °C with 5%  $\text{CO}_2$ . In DMEM, various concentrations of encapsulated betanin (S-BT) and betanin (BT) were prepared. The compounds were added

in triplicates to the designated wells and incubated for 48 h. Following the incubation time, 20 µl of 5 mg/ml MTT was added to each well and the mixture was incubated at 37 °C with 5% CO<sub>2</sub>. Following a 24 h incubation period, 100 µl of DMSO was added to each well in order to dissolve the purple formazan crystals. A thermostatically controlled plate holder, equipped with a UV–visible absorbance microplate reader (Barsamax elisa microplate reader, Molecular device, Inc., Sunnyval, CA, USA) was used to read the plate at 570 nm after a brief incubation period. The percentage of cell survival was calculated based on the following formula

$$\text{Percentage Survival} = (\text{OD of Control well} - \text{OD of blank}) / \text{OD of test well} * 100$$

### Morphological analysis

About  $6 \times 10^3$  cells were seeded per well in flat bottom 96-well plates for a duration of 24 h. After adding IC<sub>50</sub> doses of BT and S-BT, the cells were incubated for 24 h. A fluorescence microscope (Olympus) fitted with a digital imaging system was used to observe and record morphological changes in control and treated BT and S-BT.

### Detection of apoptosis by AO/EB staining

To discern the morphological indicators of apoptosis, Acridine Orange/Ethidium Bromide (AO/EB) staining was employed. SW480 cells were distributed into 24-well plates and subjected to a 24 h treatment with BT and S-BT at an IC<sub>50</sub> concentration, followed by a phosphate-buffered saline (PBS) wash and trypsinization. Immediately preceding microscopy, a mixture of 100 µl of Acridine Orange/Ethidium Bromide solution (comprising one part of 20 µl/ml Acridine Orange and 10 µg/ml Ethidium Bromide in PBS) was added. Subsequently, the cells were examined using an Olympus fluorescence microscope equipped with a digital imaging system.

### Evaluation of nuclear morphology

Using fluorescence microscopy, the DAPI-stained cell nucleus' morphology was assessed. Following the procedure, the cells were resuspended in 100 µl DAPI, fixed with ice-cold 70% ethanol, and incubated for 5 min at 37 °C while covered in aluminium foil. The cells were washed with PBS (pH 7.4). After washing the cells in PBS, they were viewed

using an Olympus fluorescence microscope that had a digital imaging system.

### Intercellular reactive oxygen species (ROS) imaging

To measure intercellular ROS production, (DCFDA), an oxidative sensitive fluorescent probe, was utilised. To find out how ROS contribute to cytotoxicity, a qualitative fluorescence microscopic study was conducted using 2'-7' Dichlorodihydrofluorescein diacetate (DCFDA), an oxidative-sensitive fluorescent probe. In short, a 24-well plate containing  $0.2 \times 10^6$  cells was pre-cultured for 24 h in DMEM. The cells were then exposed to a pre-set dose of BT and S-BT for another 24 h. After the cells were incubated, they were washed with PBS before being stained for 30 min at 37 °C in the dark using 10 mM DCFDA. The cells were washed using cold PBS. Using a fluorescence microscope, stain-positive areas were examined and captured on camera.

### Observation of mitochondrial membrane potential by Rhodamine 123

The polarised mitochondrial membrane of normal cells becomes clumped with the fluorescent dye Rhodamine 123 (Rh123). Metabolically active mitochondria are bound by this cationic dye. For 30 min, BT and S-BT treated cells were incubated with 10 µg/ml Rh 123 at 37 °C. The cells were given one PBS wash following incubation. Using an emission filter of 534 nm and an excitation wavelength of 505 nm, fluorescence microscopy was used to measure the intensity of Rho 123 staining.

### Cell cycle analysis

Following a 24 h incubation period, cells were seeded into 6-well plates at a density of approximately  $2.5 \times 10^5$  cells per well and treated with BT and S-BT for 48 h. Subsequently, the cells were harvested, washed, and fixed in ice-cold 70% ethanol, followed by overnight storage at 4 °C. The fixed cells were then exposed to an ice-cold solution containing 15 µg/ml propidium iodide, 20 µg/ml RNase A, and 0.01% Triton-X 100 before undergoing a single wash with phosphate-buffered saline (PBS) for subsequent cell cycle analysis. Data analysis was done with CytoExpert Software (USA) and data acquisition was done with a Beckman Coulter CytoFLEX (USA).

### Wound healing assay

In each well of a 6-well plate, roughly  $1 \times 10^6$  cells were seeded, and they were left to grow until they reached full confluence. After removing the media, the 200 µl tip was

used to create a straight line of scratches or wounds in the centre of the well, and the detached cells were removed by washing with  $1\times$  PBS. Images of the wound centres were taken at 0 h, after which cells were treated with free BT and its encapsulated counterpart, nanoparticles. After the treatment, pictures were taken on a regular basis with an inverted phase-contrast microscope.

### Gelatin zymography

The activity of matrix metalloproteinase (MMP) was investigated using gelatin zymography. Fully confluent cells were treated with the  $IC_{50}$  concentrations of BT and S-BT, followed by incubation for 24 h. After incubation, each well's culture media was collected. Native polyacrylamide gel electrophoresis (PAGE) with a gelatin concentration of 10 mg/ml was performed. It was incubated in an incubation buffer for 24 h after electrophoresis and before staining. The gel was then stained with Coomassie blue staining solution and destained with destaining solution.

## Results

### Characterisation of betanin loaded SNPs

#### Particle size analysis

Particle size analysis using dynamic light scattering indicated that the average hydrodynamic diameter of the

synthesized betanin-loaded starch NPs was approximately 175 nm (Fig. 1).

#### UV spectrum analysis

UV spectrum analysis differentiated the absorbance peaks of betanin (BT) and betanin-loaded SNPs (S-BT), with BT showing maximum absorbance at 538 nm and S-BT at 625 nm (Fig. 2). This shift in absorbance peak can be indicative of the interaction between betanin and the starch nanoparticles, potentially affecting the electronic structure of the betanin molecule.

#### Scanning electron microscopy imaging

SEM study revealed unambiguous morphology of spherically shaped NPs at  $20,000\times$  magnification with betanin-loaded starch NPs (Fig. 3).

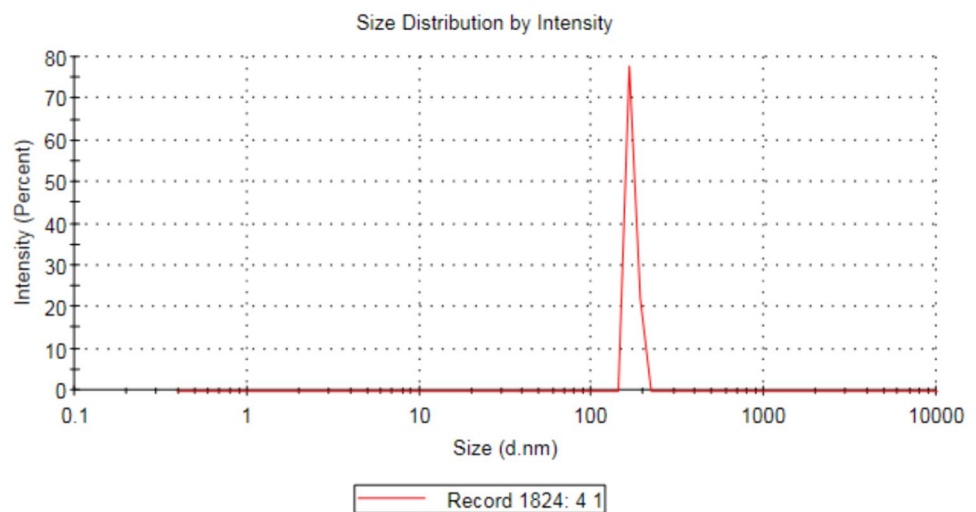
#### X-ray diffraction analysis (XRD)

X-ray diffraction analysis revealed that betanin loaded SNPs exhibited a peak range between 10 and 25 wavelength, which is characteristic of an amorphous material (Fig. 4). The amorphous nature can influence the dissolution rate and bioavailability of the encapsulated drug.

#### X-ray photoelectric spectroscopy (XPS)

Utilizing X-ray photoelectron spectroscopy (XPS), a surface-sensitive quantitative spectroscopic technique grounded in the photoelectric effect, we successfully identified the elemental composition—carbon and oxygen. This method not only discerns the elements present within the material but also provides

**Fig. 1** Particle size analysis of betanin loaded SNPs by dynamic light scattering. The mean average diameter of S-BT was found to be 175 nm





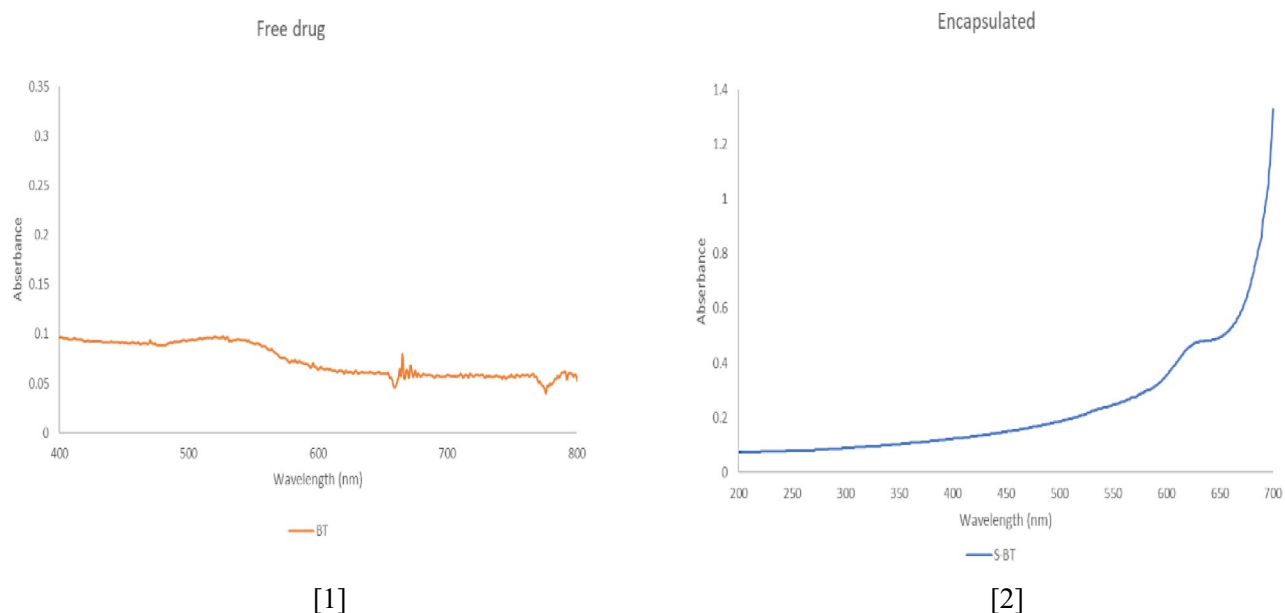
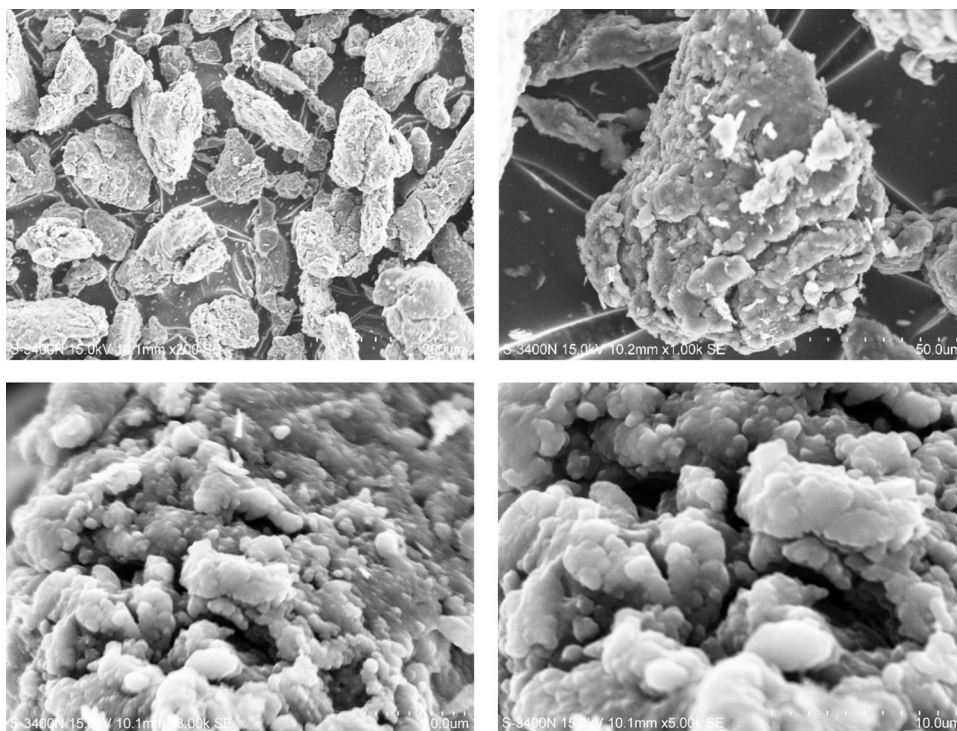


**Fig. 2** UV absorbance spectra of (1) betanin, (2) betanin loaded SNPs

**Fig. 3** SEM image of the betanin loaded SNPs showing the spherical shape of the compound



crucial insights into their chemical states, overall electronic structure and the density of electronic states within the material. The XPS analysis of S-BT yielded two distinctive spectra, portraying the elemental composition of carbon and oxygen, thereby contributing valuable information to the comprehensive characterization of the material's surface properties (Fig. 5).

### FTIR study

The FTIR spectrum of starch nanoparticles showed distinctive peaks at  $3400\text{ cm}^{-1}$ ,  $2930\text{ cm}^{-1}$  and  $1640\text{ cm}^{-1}$  that are attributed to intra and inter-molecular hydrogen bonded OH groups, C-H stretching and tightly bound water molecules,

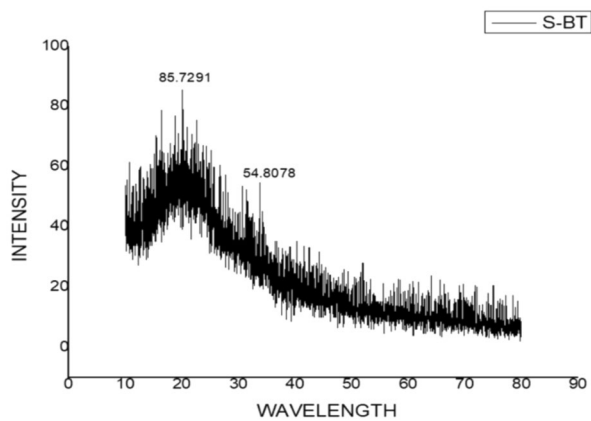


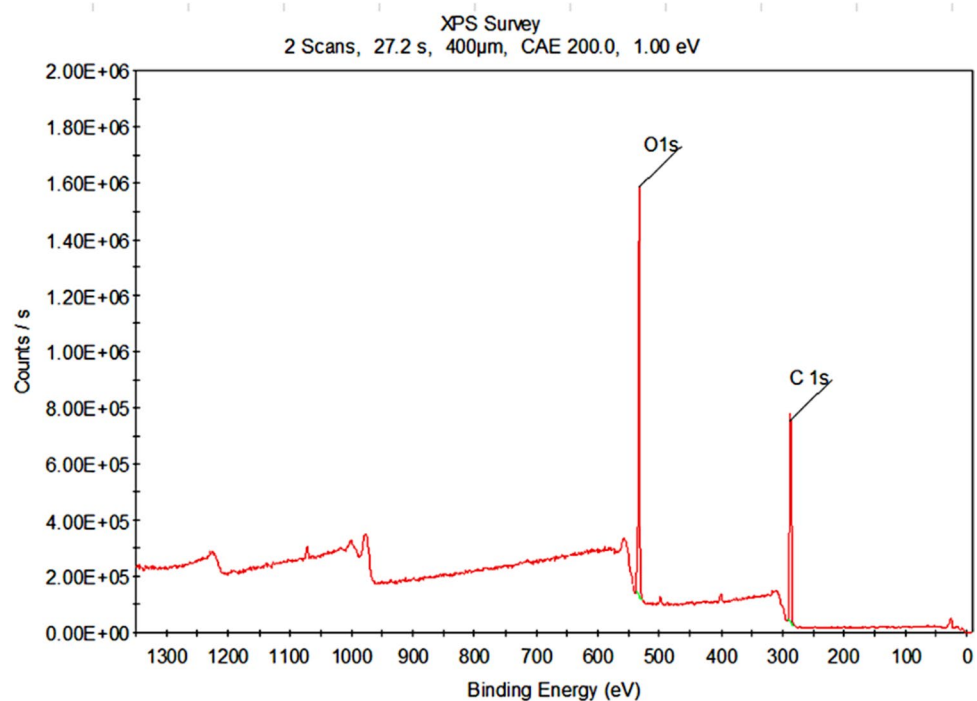
**Fig. 4** XRD graph intensity plots against Bragg's angle ranging from 10° to 80° of betanin loaded SNPs

respectively (Fig. 6). In case of S-BT, there was a shift in the band to  $3519\text{ cm}^{-1}$  due to the formation of hydrogen bonds.

#### In vitro drug release study

In vitro release of the drug from Starch NPs was evaluated by the dialysis technique. It has been observed that in 24 h, there was 13.25% of drug release. When the dialysis was carried out for 120 h (5 days), around half (42.57%) of the drug was released (Fig. 7).

**Fig. 5** Elemental composition of the betanin loaded starch NPs. The XPS survey scan shows the peak of carbon and oxygen



#### Encapsulation efficiency (%EE) and loading capacity

The amount of the free drug in the supernatant was found to be 0.866 mg. The difference of the amount of the drug used and the free untreated drug gave the amount of drug being encapsulated. The encapsulation efficiency (% EE) was found to be 99.71%. Loading capacity (% LC) was found to be 83.7%.

#### Anticancer study

##### Cell viability/cytotoxicity assay

To investigate the cytotoxic activity of BT and S-BT on colon cancer cell lines (SW480), breast cancer cell lines (MBA MD 231) and lung cancer cell lines (A549), cells were seeded into wells of 96-well culture plates. The ability of BT and S-BT to inhibit SW480, MDA MB231, and A549 cancer cells lines were analyzed using the MTT assay. The cytotoxic effect of BT and S-BT were evaluated by exposing SW480, MDA MB231, and A549 to five different concentrations (25 µg/ml, 50 µg/ml, 100 µg/ml, 200 µg/ml) for 24 h. The result showed that the cytotoxicity increased with increase in concentration of BT and S-BT. However, BT and S-BT both showed a higher level of cytotoxicity to SW480 and their  $IC_{50}$  was found to be 95 µg/ml and 42 µg/ml, respectively (Fig. 8).

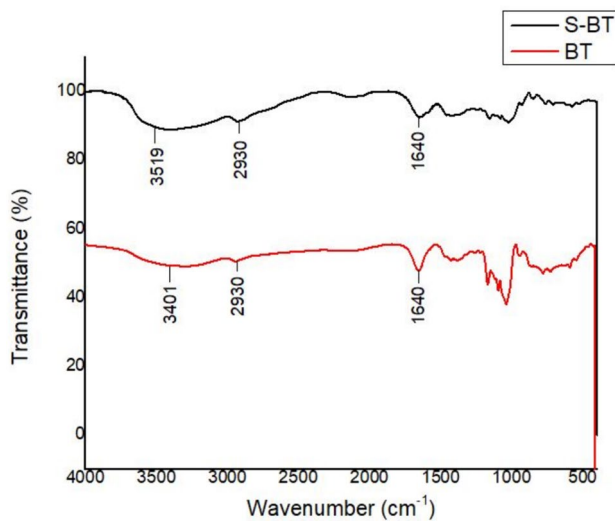


**Fig. 6** FTIR spectra of Betanin (BT) and starch encapsulated betanin (S-BT) by using KBr pellet technique

### Morphological analysis

SW480 cells were seeded in 96-well plate at about  $6 \times 10^3$  cells per well for 24 h. Wells were treated with the  $IC_{50}$

doses of BT and S-BT followed by incubation for 24 h. The results showed there was a vital loss of cells and cell death in the treated wells. Morphological changes were observed in the BT and S-BT-treated cells. S-BT-treated cells showed increased cell death (Fig. 9).

### Detection of apoptosis by AO/EB staining

The investigation into the nuclear morphology of apoptotic cells was conducted using Acridine Orange/Ethidium Bromide (AO/EB) staining. Acridine Orange (AO), a vital dye with the ability to stain both living and dead cells, and Ethidium Bromide (EB), which stains cells with compromised cell membranes, were employed in this dual staining method. The stained nuclei revealed distinct patterns: green signifying healthy cells, yellow indicating early apoptotic cells and orange/red denoting late apoptotic cells. Untreated cells exhibited uniformly green nuclei, while cells treated with BT and S-BT displayed a comparable yellow (early apoptotic) and orange/red (late apoptotic) staining profile (Fig. 10). This outcome conclusively substantiates that both BT and S-BT-induced apoptosis in SW480 colon cancer cell lines, providing valuable insights into the apoptotic response of these cells to the treatments.

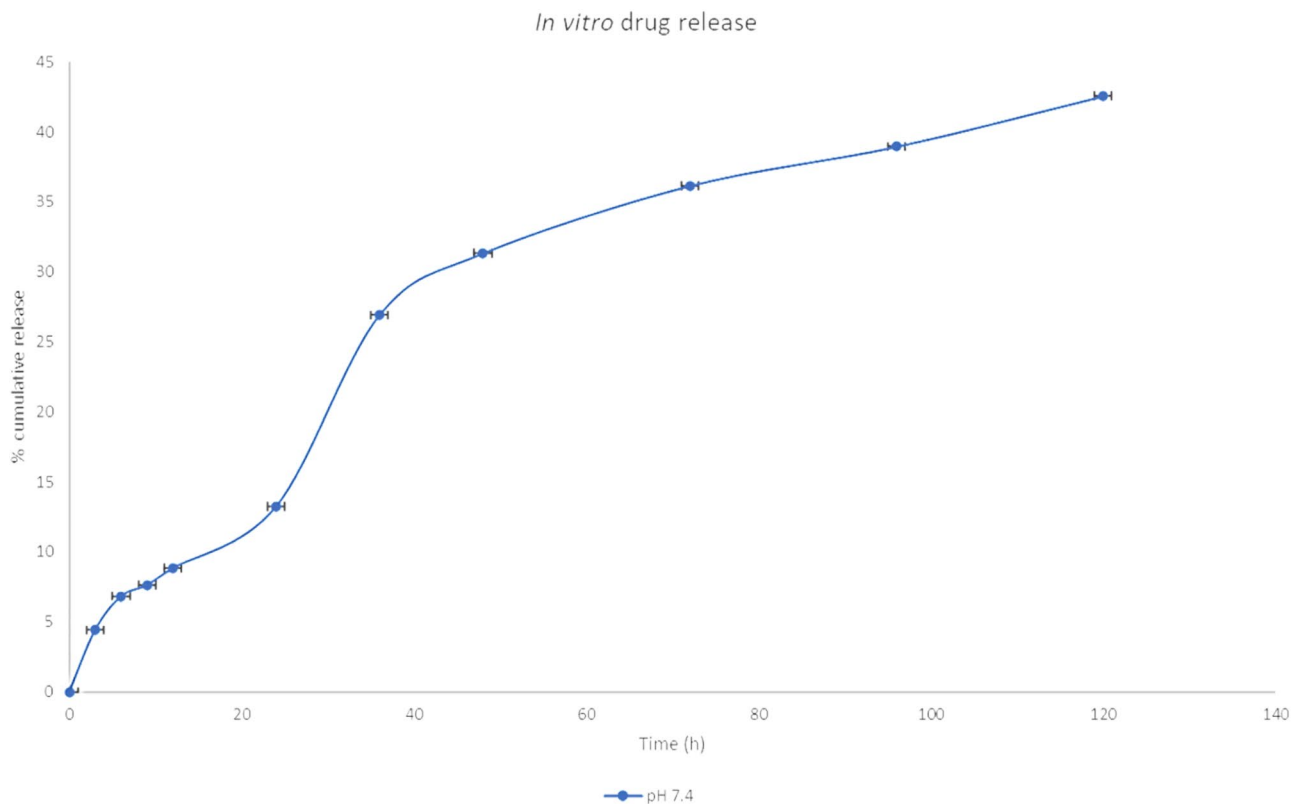


**Fig. 7** In vitro release profile of betanin from starch nanoparticles at 37°C in PBS at PH 7.4 for 120 h



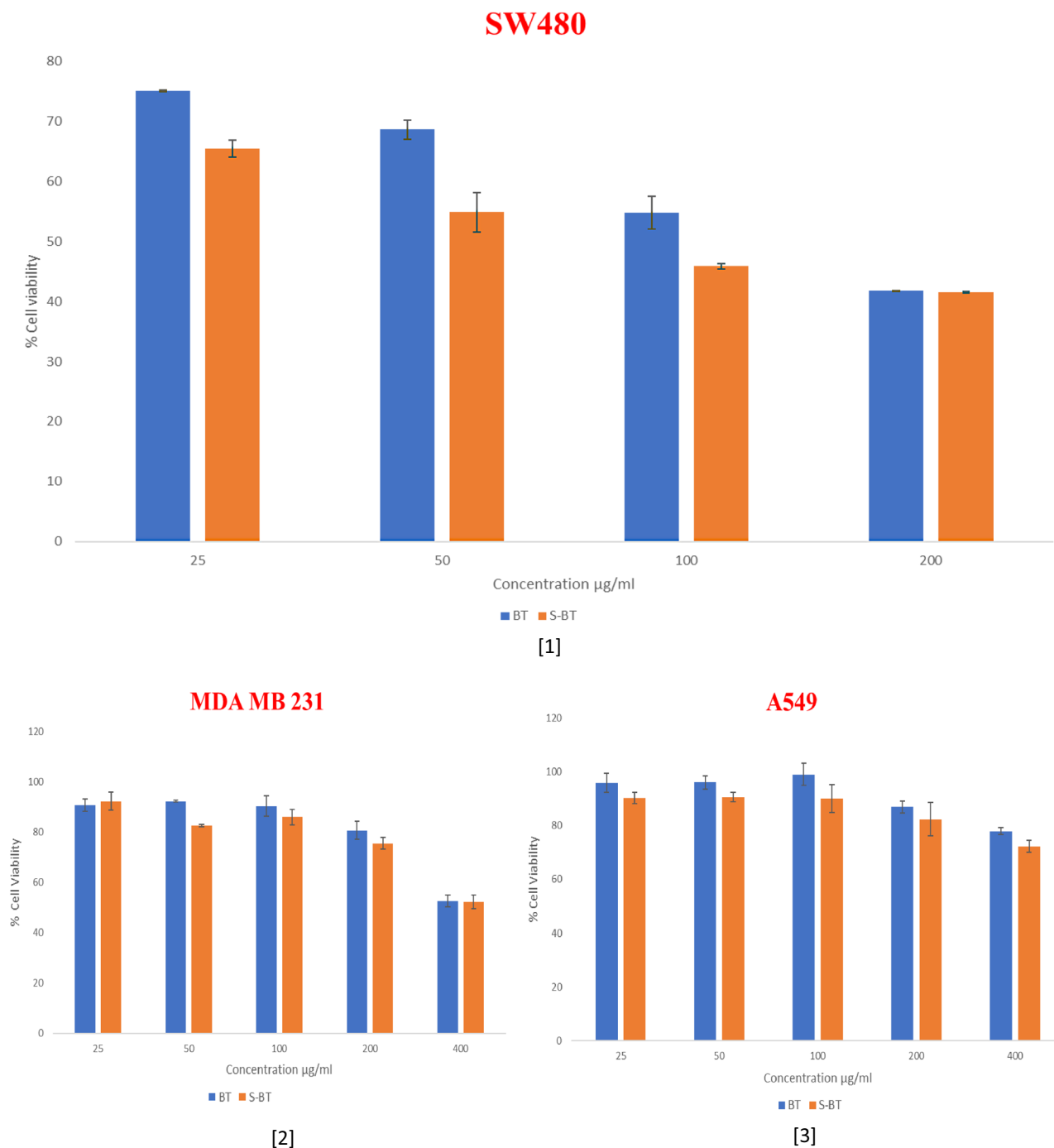


**Fig. 8** Cytotoxicity of BT and S-BT on the proliferation of (1) SW480 colon cancer cells (2) MDA MB 231 breast cancer cells and (3) A549 lung cancer cell line at 24h incubation

### Evaluation of nuclear morphology

DAPI staining was done to visualize the nuclear DNA in both live and dead cell. It is helpful to detect number of nuclei and to study cell morphology. In this study, untreated cells showed normal morphology, however, the treated cells showed nuclear condensation (Fig. 11). These characteristics

are indicative of cell apoptosis. Hence, BT and S-BT both induced apoptosis in treated cells.

### Intercellular reactive oxygen species (ROS) imaging

The maintenance of cellular homeostasis can be disrupted by various factors such as environmental stress and disease

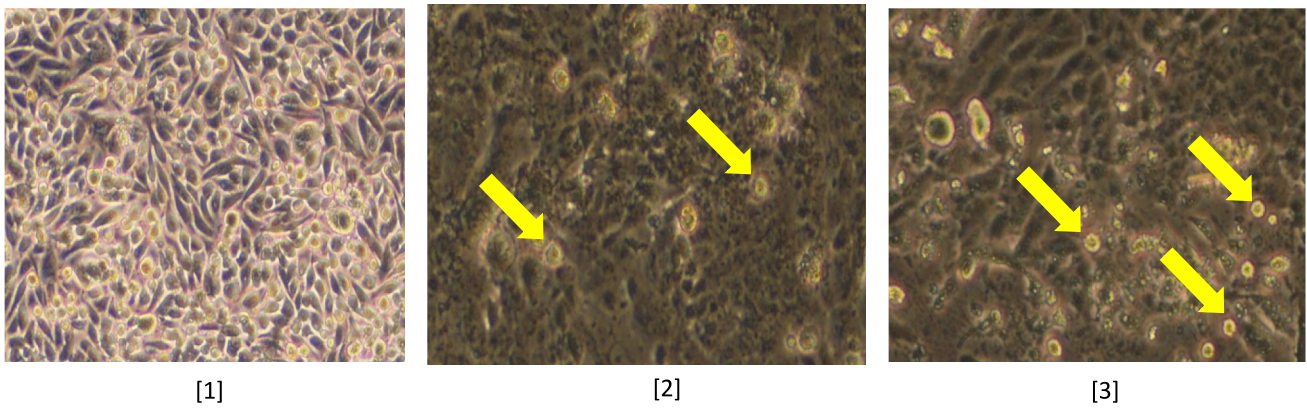


**Fig. 9** Morphological analysis of SW480 cells. (1) untreated cells, (2) BT treated cells and (3) S-BT treated cells. The visible changes like cell shrinkage and also loss of normal morphology can be seen in both treated groups

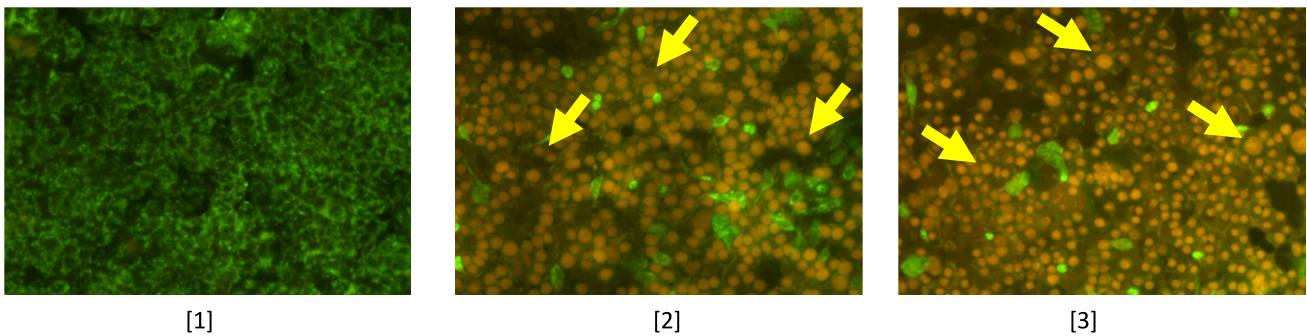


**Fig. 10** Cellular staining of SW480 cell lines, (1) untreated cells, (2) BT treated and (3) S-BT treated cells using AO/EB. The arrows indicate cell shrinkage, nuclear fragmentation, all associated with apoptotic mode of cell death

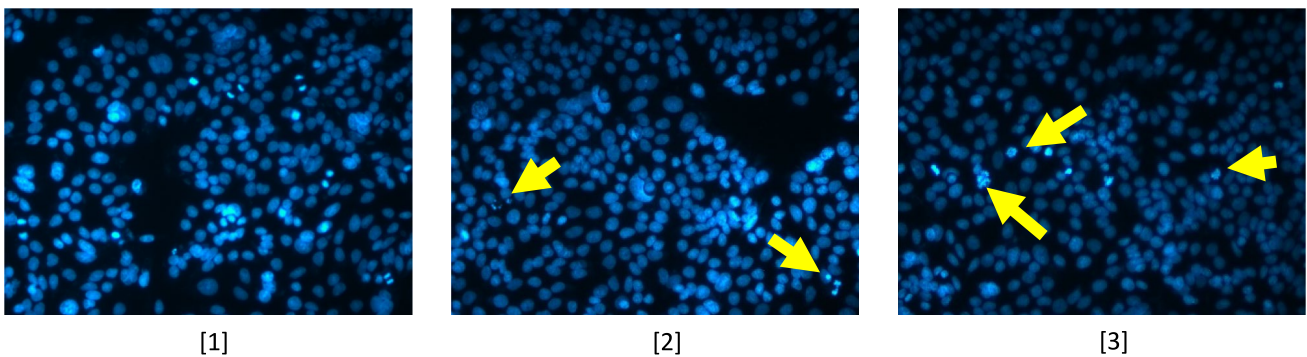


**Fig. 11** Nuclear staining using DAPI of human colon cancer cell SW480. (1) Control cells. No nuclear damage can be seen in the control cells, (2) BT treatment (3) S-BT treatment. Arrows indicate nuclear condensation of the treated cells

conditions, leading to the formation of reactive oxygen species (ROS). The formation of ROS is considered as an indicator of apoptosis. In this study, the assessment of intracellular ROS formation was conducted and it was observed that the fluorescent intensity was directly

proportional to the concentration of ROS within the cells. Treated cells exhibited a notably higher fluorescence intensity compared to untreated cells, signifying an increased concentration of intracellular ROS in the treated group (Fig. 12). This finding unequivocally establishes that both

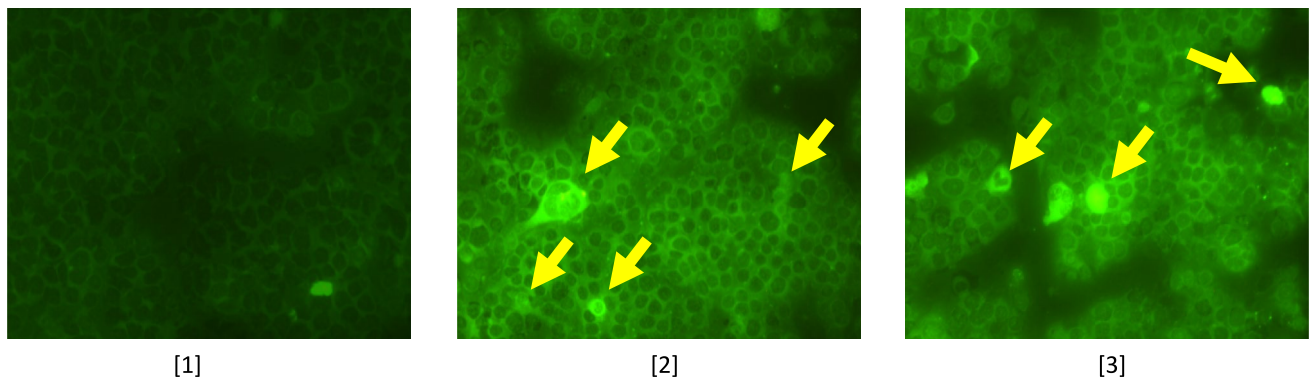


**Fig. 12** DCFDA staining for ROS generation of human colon cancer cell line SW480. (1) Control cells, (2) BT treated cells, (3) S-BT treated cells. The arrows indicate generation of ROS, indicative of apoptosis

BT and S-BT-induced apoptosis, as evidenced by the substantial elevation in ROS production in the treated cells compared to their untreated counterparts. This observation provides valuable insights into the mechanistic aspects of apoptosis induction by BT and S-BT.

#### Observation of mitochondrial membrane potential by Rhodamine 123

Mitochondrial membrane potential is a key indicator to measure mitochondrial function. Decrease in mitochondrial membrane potential usually indicates apoptosis. Rhodamine 123 dye is cell permanent dye. The fluorescence intensity is proportional to the amount of dye that enters the cell. Here, we can observe more fluorescence intensity in untreated cells than treated (Fig. 13). This indicates that there was loss of function of mitochondria in treated cells, which led to apoptosis. Hence, BT and S-BT-induced apoptosis in treated cells.

#### Cell cycle analysis

FACS or fluorescence activated cell sorting counts the total number of cells present in each phase of the cell cycle. Cells were treated with the  $IC_{50}$  drug concentration and incubated for 24 h. The cells were then fixated in 70% ethanol. FACS was used to count both untreated and treated cells stained with Propidium iodide. In our research, we observed the accumulation of cells in the G2-M phase of the cell cycle (Fig. 14). This implies that the treated cells were arrested in the G2-M phase. Thus, both the compounds prevented the cancer progression by stopping the cell cycle in the G2-M phase.

#### Wound healing assay

In a six-well plate, cells were grown nearly to confluence before being wound. In less than 24 h, culture cells were able to grow, migrate and close the wound. However, addition of the plain drug and the encapsulated drug resulted in wound closure inhibition after 24 h, indicating that the drug and

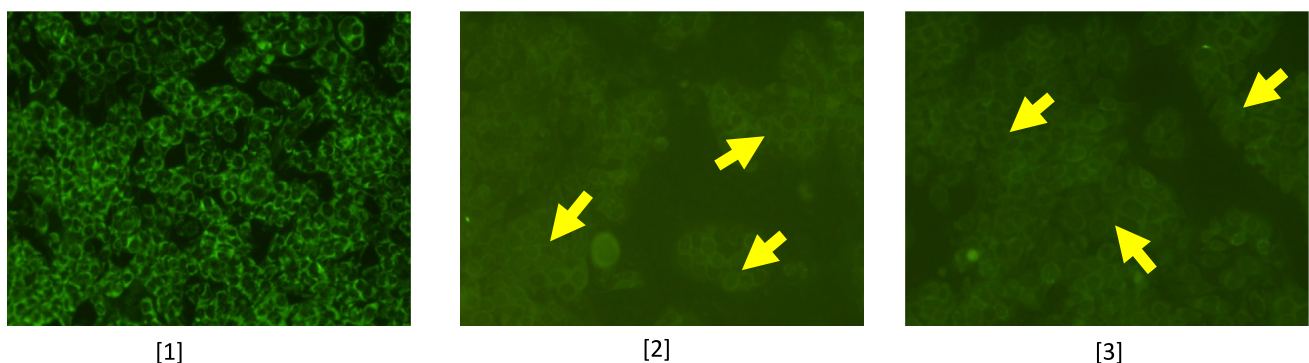


**Fig. 13** Mitochondrial staining using Rhodamine 123 on (1) Control SW480 cells, (2) BT treated cells, (3) S-BT treated SW480 cell lines. The arrows indicate loss of mitochondrial membrane potential



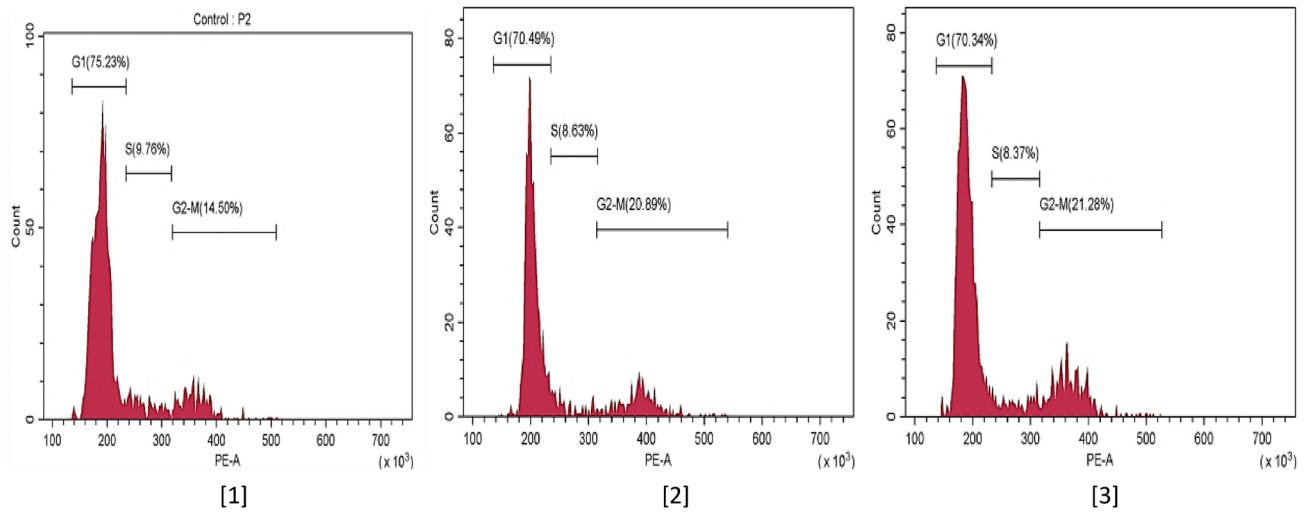


**Fig. 14** Cell cycle analysis by FACS. Cells were found to be arrested in G2-M phase. (1) Control cell (2) BT treated cells (3) S-BT treated cells

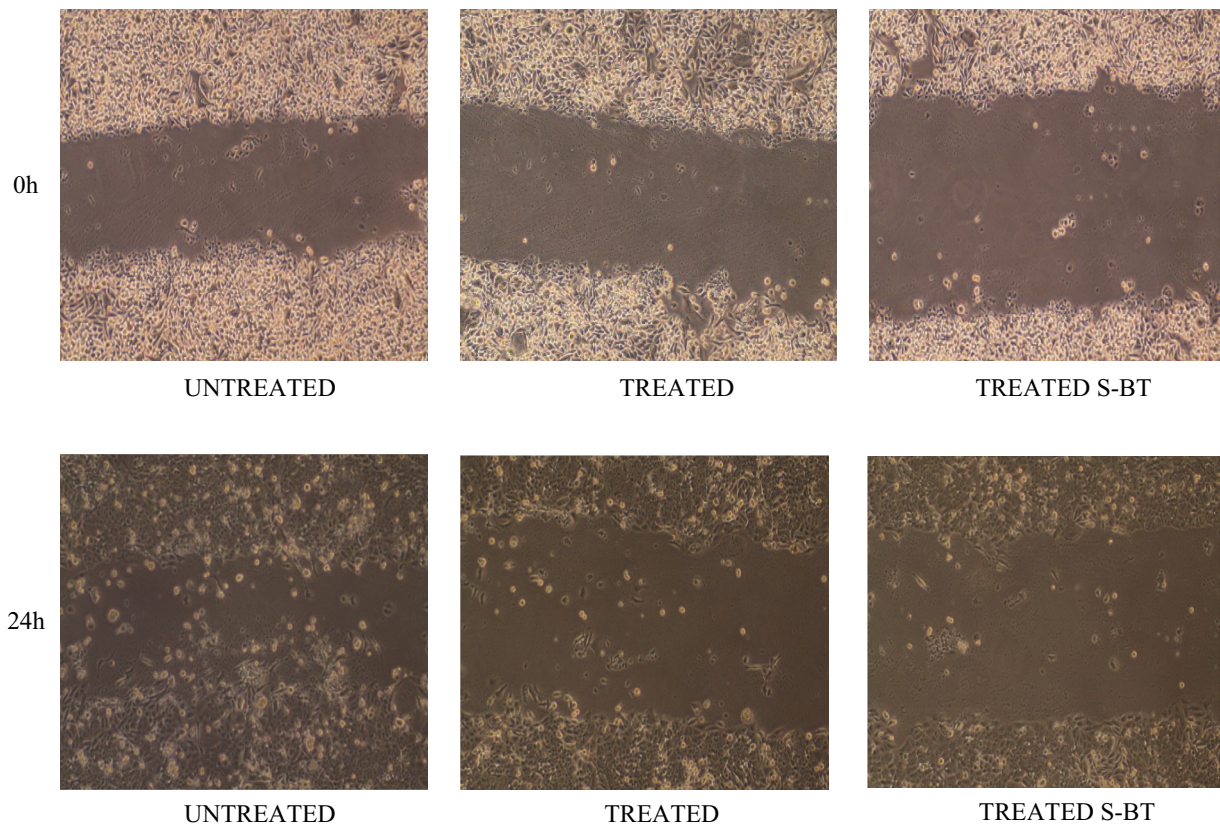


**Fig. 15** Wound healing assay. After the scratches (wounds) were made, time-dependent images were obtained. The wound closed within 24h in the control group, but it remained nearly same in the treated group

drug loaded SNPs inhibited cell migration when compared to control (Fig. 15).

### Gelatin zymography

The activity of matrix metalloproteinases (MMP's) were studied using gelatin zymography. In comparison to untreated group, treated group developed a faint band indicating that the levels of MMPs were decreased as shown in Fig. 16.

### Discussion

The anticancer efficacy and characterization of starch nanoparticles (SNPs) loaded with betanin were thoroughly examined in this study. The mean particle size of betanin loaded nanoparticles was found to be 175 nm (Hanahan and Weinberg 2011). The UV spectrum analysis showed that the

maximum absorbance of the encapsulated form shifted from 538 nm for free betanin to 625 nm for the encapsulated form, suggesting that the chemical environment of the betanin may have changed during encapsulation (Wang et al. 2019). The successful synthesis of betanin-loaded SNPs was confirmed by images captured by scanning electron microscopy, which clearly showed the spherical shaped nanoparticles.

An amorphous structural characteristic of the nanoparticles was revealed by the X-ray diffraction analysis, which may help with drug release kinetics (Kothamasu et al. 2012). The presence of carbon and oxygen was further verified by X-ray photoelectron spectroscopy, suggesting that the betanin was successfully encapsulated within the SNPs and was pure. The FTIR spectroscopy was done to evaluate the interaction between betanin and starch nanoparticles. The FTIR spectrum of starch nanoparticles showed distinctive peaks at  $3400\text{ cm}^{-1}$  (inter- and intramolecular hydrogen-bonded hydroxyl groups),  $2930\text{ cm}^{-1}$  and  $1640\text{ cm}^{-1}$  (C–H stretching and water molecules in starch) as described in the previous literature (Liu et al. 2017). A shift in the band peak from  $3400$  to  $3519\text{ cm}^{-1}$  due to the formation of hydrogen bonds confirmed the successful encapsulation of betanin in the starch nanoparticles (Kumar et al. 2014).

The sustained release allows the delivery of a drug at a rate that leads its delivery for a longer period of time. The concentration of a drug can be kept at constant levels in tissue or blood by allowing the drug to be released at sustained manner (Shah et al. 2019). The extended release of a drug from the nanoparticles can achieve higher degree of targeting, thereby increasing the efficacy of the drug (Kalaydina et al. 2018). About 42.57% of the drug was released during the 120 h controlled release observed in the in vitro release study. This is a desirable feature for sustained drug delivery systems.

With an encapsulation efficiency of 99.71% and a loading capacity of 83.7%, respectively, these results demonstrate an effective drug delivery system (Joudeh and Linke 2022). Using the MTT assay, the cytotoxic activity of both free betanin (BT) and encapsulated betanin (S-BT) on different cancer cell lines (Ninfali and Angelino 2013; Stryker et al. 1987) was analysed. As seen by their respective  $IC_{50}$  values, the results showed a concentration-dependent increase in cytotoxicity, with S-BT exhibiting greater cytotoxicity to SW480 cells than BT.

These conclusions were supported by morphological analysis using fluorescence images, which demonstrated notable morphological changes and cell death following treatment with  $IC_{50}$  doses of BT and S-BT. By showing the presence of early and late apoptotic cells after treatment, AO/EB staining verified that these compounds could cause apoptosis. Further evidence of this apoptotic induction came from DAPI staining, which showed the nuclear condensation typical of apoptosis and elevated levels of reactive oxygen

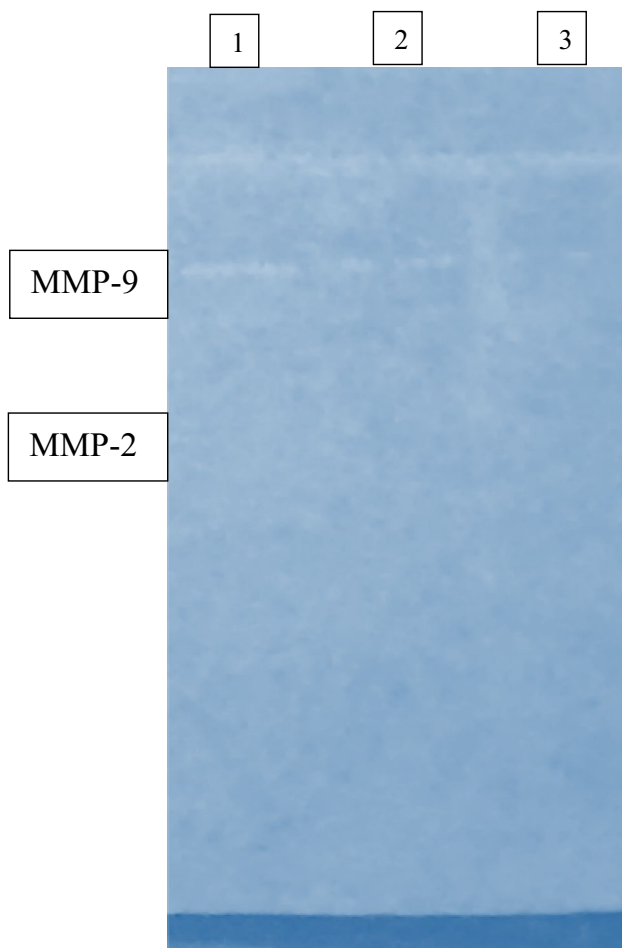


**Fig. 16** Evaluation of MMP activity in SW480 colon cancer cells. (1) untreated SW480 cells, (2) and (3) are SW480 cells treated with  $IC_{50}$  dose of BT and S-BT, respectively



species in treated cells—a known inducer of apoptotic pathways (Mahmoudi Najafi et al. 2016).

Additionally, a reduction in the potential of the mitochondrial membrane as revealed by Rhodamine 123 staining indicated a loss of mitochondrial function that resulted in apoptosis (Trucillo et al. 2018). The cell cycle analysis revealed the arrest of cells in the G2-M phase of the cell cycle, which revealed the role of betanin as an anticancer agent (El-Naggar et al. 2015).

The drug's anti-metastatic property was demonstrated by the wound healing assay, which revealed reduced cell migration in treated groups relative to control (Marques et al. 2002). Finally, compared to untreated control, gelatin zymography demonstrated lower matrix metalloproteinase activity in the treated cells, an important factor in the extracellular matrix's breakdown during metastasis (Pandolfi 2001; Ren et al. 2017).

In conclusion, the thorough characterization and anticancer investigations offered in this study provide compelling evidence for the potential of betanin and betanin encapsulated starch as potent anticancer agents, able to induce apoptosis, cytotoxicity and inhibition of cancer cell metastases. S-BT is an attractive candidate for cancer therapy due to its high encapsulation efficiency and sustained release profile, which calls for more research and development.

**Acknowledgements** The authors acknowledge the central instrumentation facility (Pondicherry University), DST-FIST for providing the required facilities and infrastructure.

**Author contributions** Conceived and designed the analysis—RR; collected the data—SC, SAB, CH; contributed data or analysis tools—SAB, SC, SP; paper writing and editing—SC, GSK and RR, resources—ASN, DM.

**Funding** The authors declare that no funds or any other support were received during preparation of this manuscript.

**Data availability** The data used to support the findings of this study are available from corresponding author upon request.

## Declarations

**Conflict of interest** The authors have no conflict of interests to declare.

**Informed consent** Not applicable.

**Research involving human participants and/or animals** Not applicable.

## References

Aztatzi-Ruggerio L, Granados-Balbuena SY, Zainos-Cuapio Y, Ocaranza-Sánchez E, Rojas-López M (2019) Analysis of the degradation of betanin obtained from beetroot using Fourier transform infrared spectroscopy. *J Food Sci Technol* 56:3677–3686. <https://doi.org/10.1007/s13197-019-03826-2>

- Bray F, Ferlay J, Soerjomataram I, Siegel RL, Torre LA, Jemal A (2018) Global cancer statistics 2018: GLOBOCAN estimates of incidence and mortality worldwide for 36 cancers in 185 countries. *CA Cancer J Clin* 68:394–424. <https://doi.org/10.3322/caac.21492>
- Chen Z, Fu Z, Li L, Ma E, Guo X (2021) A cost-effective nano-sized curcumin delivery system with high drug loading capacity prepared via flash nanoprecipitation. *Nanomaterials* 11:734. <https://doi.org/10.3390/nano11030734>
- Chen J, Karmakar B, Salem MA, Alzahrani AY, Bani-Fwaz MZ, Abdel-Daim MM, El-kott AF (2022) CuO NPs@Starch as a novel chemotherapeutic drug for the treatment of several types of gastrointestinal system cancers including gastric, pancreatic, and colon cancers. *Arab J Chem* 15:103681. <https://doi.org/10.1016/j.arabjc.2021.103681>
- Contreras-Cáceres R, Cabeza L, Perazzoli G, Díaz A, López-Romero JM, Melguizo C, Prados J (2019) Electrospun nanofibers: recent applications in drug delivery and cancer therapy. *Nanomaterials* 9:656. <https://doi.org/10.3390/nano9040656>
- Da Silva DVT, Baião DDS, De Oliveira Silva F, Alves G, Perrone D, Del Aguila EM, Paschoalin VMF (2019) Betanin, a natural food additive: stability, bioavailability, antioxidant and preservative ability assessments. *Molecules* 24:458. <https://doi.org/10.3390/molecules24030458>
- El-Naggar ME, El-Rafie MH, El-sheikh MA, El-Feky GS, Hebeish A (2015) Synthesis, characterization, release kinetics and toxicity profile of drug-loaded starch nanoparticles. *Int J Biol Macromol* 81:718–729. <https://doi.org/10.1016/j.ijbiomac.2015.09.005>
- Hanahan D, Weinberg RA (2011) Hallmarks of cancer: the next generation. *Cell* 144:646–674. <https://doi.org/10.1016/j.cell.2011.02.013>
- Hossain MdS, Karuniawati H, Jairoun AA, Urbi Z, Ooi DJ, John A, Lim YC, Kibria KMK, Mohiuddin AKM, Ming LC, Goh KW, Hadi MA (2022) Colorectal cancer: a review of carcinogenesis, global epidemiology, current challenges, risk factors, preventive and treatment strategies. *Cancers* 14:1732. <https://doi.org/10.3390/cancers14071732>
- Jimenez RE, Hartwig W, Antoniu BA, Compton CC, Warshaw AL, Fernández-del Castillo C (2000) Effect of matrix metalloproteinase inhibition on pancreatic cancer invasion and metastasis: an additive strategy for cancer control. *Ann Surg* 231:644–654. <https://doi.org/10.1097/0000658-200005000-00004>
- Joudeh N, Linke D (2022) Nanoparticle classification, physicochemical properties, characterization, and applications: a comprehensive review for biologists. *J Nanobiotechnol* 20:262. <https://doi.org/10.1186/s12951-022-01477-8>
- Kalaydina R, Bajwa K, Qorri B, DeCarlo A, Szewczuk MR (2018) Recent advances in “smart” delivery systems for extended drug release in cancer therapy. *Int J Nanomed* 13:4727–4745. <https://doi.org/10.2147/ijn.s168053>
- Kapadia GJ, Azuine MA, Rao GS, Arai T, Iida A, Tokuda H (2011) Cytotoxic effect of the red beetroot (*Beta vulgaris* L.) extract compared to doxorubicin (Adriamycin) in the human prostate (PC-3) and breast (MCF-7) cancer cell lines. *Anticancer Agents Med Chem* 11:280–284. <https://doi.org/10.2174/187152011795347504>
- Khan MI (2015) Plant betalains: safety, antioxidant activity, clinical efficacy, and bioavailability. *Compr Rev Food Sci Food Saf* 15:316–330. <https://doi.org/10.1111/1541-4337.12185>
- Kothamasu P, Kanumur H, Ravur N, Maddu C, Parasuramrajam R, Thangavel S (2012) Nanocapsules: the weapons for novel drug delivery systems. *BioImpacts* 2:71–81. <https://doi.org/10.5681/bi.2012.011>
- Kumar P, Senthamilselvi S, Govindaraju M (2014) Phloroglucinol-encapsulated starch biopolymer: preparation, antioxidant and cytotoxic effects on HepG2 liver cancer cell lines. *RSC Adv* 4:26787. <https://doi.org/10.1039/c4ra02621g>

- Liu C, Li M, Ji N, Liu J, Xiong L, Sun Q (2017) Morphology and characteristics of starch nanoparticles self-assembled via a rapid ultrasonication method for peppermint oil encapsulation. *J Agric Food Chem* 65:8363–8373. <https://doi.org/10.1021/acs.jafc.7b02938>
- Lu J, Wu L, Wang X, Zhu J, Du J, Shen B (2018) Detection of mitochondria membrane potential to study CLIC4 knockdown-induced HN4 cell apoptosis in vitro. *J vis Exp* 137:56317. <https://doi.org/10.3791/56317>
- Mahmoudi Najafi SH, Baghaie M, Ashori A (2016) Preparation and characterization of acetylated starch nanoparticles as drug carrier: ciprofloxacin as a model. *Int J Biol Macromol* 87:48–54. <https://doi.org/10.1016/j.ijbiomac.2016.02.030>
- Marques AP, Reis RL, Hunt JA (2002) The biocompatibility of novel starch-based polymers and composites: in vitro studies. *Biomaterials* 23:1471–1478. [https://doi.org/10.1016/S0142-9612\(01\)00272-1](https://doi.org/10.1016/S0142-9612(01)00272-1)
- Mourdikoudis S, Pallares RM, Thanh NTK (2018) Characterization techniques for nanoparticles: comparison and complementarity upon studying nanoparticle properties. *Nanoscale* 10:12871–12934. <https://doi.org/10.1039/C8NR02278J>
- Ninfali P, Angelino D (2013) Nutritional and functional potential of *Beta vulgaris cicla* and *rubra*. *Fitoterapia* 89:188–199. <https://doi.org/10.1016/j.fitote.2013.06.004>
- Otto T, Sicinski P (2017) Cell cycle proteins as promising targets in cancer therapy. *Nat Rev Cancer* 17:93–115. <https://doi.org/10.1038/nrc.2016.138>
- Paini M, Daly SR, Aliakbarian B, Fathi A, Tehrani EA, Perego P, Dehghani F, Valtchev P (2015) An efficient liposome based method for antioxidants encapsulation. *Colloids Surf, B* 136:1067–1072. <https://doi.org/10.1016/j.colsurfb.2015.10.038>
- Pandolfi PP (2001) Transcription therapy for cancer. *Oncogene* 20(24):3116–3127. <https://doi.org/10.1038/sj.onc.1204299>
- Pang SC, Chin SF, Nadirah A, Tay SH, Mohd Yazid SNA (2015) Fabrication of polysaccharide-based nanoparticles as drug delivery nanocarriers. *ECS Trans* 66:15–32. <https://doi.org/10.1149/06637.0015ecst>
- Pickhardt PJ, Kim DH, Pooler BD, Hinshaw JL, Barlow D, Jensen D, Reichelderfer M, Cash BD (2013) Assessment of volumetric growth rates of small colorectal polyps with CT colonography: a longitudinal study of natural history. *Lancet Oncol* 14:711–720. [https://doi.org/10.1016/S1470-2045\(13\)70216-X](https://doi.org/10.1016/S1470-2045(13)70216-X)
- Ren Z, Chen J, Khalil RA (2017) Zymography as a research tool in the study of matrix metalloproteinase inhibitors. *Methods Mol Biol* 1626:79–102. [https://doi.org/10.1007/978-1-4939-7111-4\\_8](https://doi.org/10.1007/978-1-4939-7111-4_8)
- Richon VM, Emiliani S, Verdin E, Webb Y, Breslow R, Rifkind RA, Marks PA (1998) A class of hybrid polar inducers of transformed cell differentiation inhibits histone deacetylases. *Proc Natl Acad Sci* 95:3003–3007. <https://doi.org/10.1073/pnas.95.6.3003>
- Salimi A, Bahiraei T, Ahdeno S, Vatanpour S, Pourahmad J (2021) Evaluation of cytotoxic activity of betanin against U87MG human glioma cells and normal human lymphocytes and its anticancer potential through mitochondrial pathway. *Nutr Cancer* 73:450–459. <https://doi.org/10.1080/01635581.2020.1764068>
- Shah MR, Imran M, Ullah S (2019) Nanocarrier-based targeted pulmonary delivery: novel approaches for effective lung cancer treatment. *Chemotherapy*. <https://doi.org/10.1016/b978-0-12-816773-1.00006-7>
- Siegel RL, Miller KD, Jemal A (2020) Cancer statistics, 2020. *CA Cancer J Clin* 70:7–30. <https://doi.org/10.3322/caac.21590>
- Sreekanth D, Arunasree MK, Roy KR, Chandramohan Reddy T, Reddy GV, Reddanna P (2007) Betanin a betacyanin pigment purified from fruits of *Opuntia ficus-indica* induces apoptosis in human chronic myeloid leukemia Cell line-K562. *Phytomedicine* 14:739–746. <https://doi.org/10.1016/j.phymed.2007.03.017>
- Stryker SJ, Wolff BG, Culp CE, Libbe SD, Ilstrup DM, MacCarty RL (1987) Natural history of untreated colonic polyps. *Gastroenterology* 93:1009–1013. [https://doi.org/10.1016/0016-5085\(87\)90563-4](https://doi.org/10.1016/0016-5085(87)90563-4)
- Trucillo P, Campardelli R, Reverchon E (2018) Production of liposomes loaded with antioxidants using a supercritical CO<sub>2</sub> assisted process. *Powder Technol* 323:155–162. <https://doi.org/10.1016/j.powtec.2017.10.007>
- Wang X, Decker CC, Zechner L, Krstin S, Wink M (2019) In vitro wound healing of tumor cells: inhibition of cell migration by selected cytotoxic alkaloids. *BMC Pharmacol Toxicol* 20:4. <https://doi.org/10.1186/s40360-018-0284-4>
- Wlodkowic D, Telford W, Skommer J, Darzynkiewicz Z (2011) Apoptosis and beyond: cytometry in studies of programmed cell death. *Methods Cell Biol* 103:55–98. <https://doi.org/10.1016/B978-0-12-385493-3.00004-8>
- Wu X, Chang Y, Fu Y, Ren L, Tong J, Zhou J (2016) Effects of non-solvent and starch solution on formation of starch nanoparticles by nanoprecipitation. *Starch Stärke* 68:258–263. <https://doi.org/10.1002/star.201500269>
- Xie Y-H, Chen Y-X, Fang J-Y (2020) Comprehensive review of targeted therapy for colorectal cancer. *Signal Transduct Target Ther* 5:22. <https://doi.org/10.1038/s41392-020-0116-z>
- Zaremba-Czogalla M, Jaromin A, Sidoryk K, Zagórska A, Cybulski M, Gubernator J (2020) Evaluation of the in vitro cytotoxic activity of caffeic acid derivatives and liposomal formulation against pancreatic cancer cell lines. *Materials* 13:5813. <https://doi.org/10.3390/ma13245813>

Springer Nature or its licensor (e.g. a society or other partner) holds exclusive rights to this article under a publishing agreement with the author(s) or other rightsholder(s); author self-archiving of the accepted manuscript version of this article is solely governed by the terms of such publishing agreement and applicable law.